RSC Advances

ROYAL SOCIETY OF CHEMISTRY

www.rsc.org/advances

Journal Name

ARTICLE

Viscoelastic and durability analysis of nanostructured composite layers of polyelectrolyte and nanoparticles

Kenta Fukada,[a] Taihei Taniguchi,[a] and Seimei Shiratori*[a]

Received 00th January 20xx,
Accepted 00th January 20xx

DOI: 10.1039/x0xx00000x

www.rsc.org/

We have evaluated the abrasion and bending durabilities of stacked polymer/nanoparticle layer-by-layer films. This was performed with a quartz crystal microbalance with dissipation (nondestructive test) and with independent abrasion and bending tests. We compared various films having different nanoparticle content ratios, or different vertical (depth) material distributions, with quartz crystal microbalance and glow discharge optical emission spectroscopy. We found that the decay times of quartz crystal microbalance were longer when there was an excess of nanoparticles in the film or if it was a uniform layered structure. Higher durabilities were also observed in these structures, which were correlated to the dissipation results. Thus abrasion and bending durabilities can be estimated using nondestructive method.

1. Introduction

Organic/inorganic composite films that have both mechanical durability and flexibility have been proposed for various applications. Fabrication of these films by wet processes is environmentally friendly and low-cost. Layer-by-layer (LbL)[1-6] self-assembly is one such method, and involves alternating depositions of cationic and anionic materials by electrostatic forces. For film growth control in air or in solvents, quartz crystal microbalance (QCM) methods[7-10] are frequently used[11-13]. However, it is difficult to estimate the hardness of LbL films by knowing only the concentration of cation and anion solutions and the amount of each material in the films. Durability is generally characterized by tests such as abrasion, pencil scratching, water resistance, heat resistance, and bending. However, these tests alter or destroy the films. Alternatively, the viscoelasticity of coated materials has been characterized by measuring energy dissipation with a QCM (QCM-D)[14-21]; *i.e.*, the attenuated amplitude is monitored as a function of time after shutting off the QCM power. The hardness of fabricated films can be similarly measured as a nondestructive test. For example, QCM decay times for coatings of soft materials are shorter because of cancelation effects than those made with hard materials. The voltage amplitude *V(t)* of a QCM at time *t* is given by[14-16]:

$$V(t) = Vo \times \exp\left(\frac{-t}{\tau}\right) \times \sin(2\pi f t + \varphi) \quad (1)$$

Where V_o is the amplitude of the voltage at t=0, f is the frequency obtained from fitting the damping function, τ is the decay time constant, and ϕ is the phase difference. QCM-D has been used in conjunction with ellipsometry, atomic force microscopy (AFM), and surface plasmon resonance[22-24].

Commercial QCM-D instruments (*e.g.*, Q-Sense QCM-D from Biolin Scientific) are commonly used because they have high sensitivity and enable sensing of DNA[25], RNA[26], surfactants[27,28], dyes[29], bacteria[30-32], lipids[33-35], gels[36,37], and various other organic materials[38-41]. They can also detect inorganic materials such as SiO_2 nanoparticle monolayers[42] and organic/inorganic composite films such as SiO_2/polymer LbL films[43], TiO_2/polymer LbL films[44], nanoparticle/cellulose nanofiber composite films[45], Si nanoparticle composites with PDDA[46] and Au nanoparticle composites with lipids[47].

QCM-D has been used to characterize nanoparticles in organic/inorganic composite films. The locations of nanoparticles in LbL films and the effects of thermal transitions were studied[48]. Wetting of PVDF/TiO_2 composite films having different TiO_2 content ratios were examined; however, only frequency shifts were measured[49]. To enhance the hardness of LbL films, mussel adhesive proteins and ceria nanoparticles of various concentrations in the cation and anion solutions were studied, as well as the number of bilayers[50]. Viscoelasticity was also measured by QCM-D and the abrasion resistance of the coatings was characterized with controlled-force contact mode AFM.

The robustness of organic/inorganic composite films has been studied with QCM-D. However, the relationship between film hardness and the inorganic material content ratio has not been reported. Furthermore, the relationship of viscoelasticity and abrasion or bending durability has not been examined with QCM-D. Here, we evaluated the viscoelasticity of organic/inorganic composite films with various inorganic nanoparticle content ratios by QCM, QCM-D, glow discharge optical emission spectroscopy (GDOES),[51, 52] and independent abrasion and bending tests. We fabricated the polymer/nanoparticle stacked LbL films with various nanoparticle content ratios, which were estimated by QCM and

[a] *School of Integrated Design Engineering, Center for Science and Technology for Designing Functions, Graduate School of Science and Technology, Keio University, 3-14-1 Hiyoshi, Kohoku-ku, Yokohama, Kanagawa 223-8522 Japan*
Tel: +81-45-566-1602
Fax: +81-45-566-1602
E-mail: shiratori@appi.keio.ac.jp

† Electronic Supplementary Information (ESI) available: Programs on UNIX environment for QCM-D and raw data of GDOES. See DOI: 10.1039/x0xx00000x

GDOES. We investigated the QCM frequency shifts as the polymer and nanoparticles were adsorbed, while the atomic ratios of the films were analyzed with GDOES depth profiles.

The simple QCM-D system used a digital storage oscilloscope and UNIX[53] programs for analyzing the 2×10^6 (2M) plots stored in the oscilloscope. We used Cygwin UNIX for Windows (http://www.cygwin.com, Red Hat, Inc., Raleigh, NC, USA) for large-data-set analysis techniques to obtain QCM-D frequency information and for the determination of viscoelasticities of stacked polymer/nanoparticle films. We then characterized the abrasion or bending durability of these films. By using the results from QCM, QCM-D, and GDEOS, the relationship between the layered structures or polymer/nanoparticle ratios and viscoelasticity is determined.

2. Experimental

2.1. Materials

Anti-reflection organic/inorganic composite films were fabricated with the LbL process. The following materials were used without purification. Poly(ethylene imine) (PEI, Mw=70,000, Wako Pure Chemical Industries, Ltd.) was the positively charged material, while the negatively charged materials were titanium(IV) bis(ammonium lactato) dihydroxide (TALH, 50wt% in H_2O, Sigma-Aldrich), which was the precursor of TiO_2 nanoparticles, and an aqueous dispersion of SiO_2 nanoparticles(OS, Nissan Chemical Industries, Ltd.). We used TiO_2 as a high-refractive-index material and SiO_2 as a low-refractive-index material. Poly(sodium 4-styrene sulfonate) (PSS, Mw=70,000, Sigma-Aldrich) and poly(diallyldimethylammonium-chloride) (PDDA, Mw= 200,000~350,000, 20wt% in H_2O, Sigma-Aldrich) were used as buffer layers on the QCM for stabilizing the frequency[54]. The concentrations of PEI, TALH, and SiO_2 were adjusted to 0.01 M, 1.0 wt.% and 0.2 wt.%, respectively, with ultra-pure water (>18 MΩ cm). The respective pH values were 10.2, 3.6, and 5.4.

2.2. Film fabrication

Solutions were stirred for 24 hours and used within several days. The flexible substrate indium tin oxide-polyethylene-naphthalate (ITO-PEN) was ultrasonically washed in ethanol for 5 min and twice in ultra-pure water for 5 min. When we deposited material B over material A, we defined it as (A/B). If the sequence was repeated "n" times, we defined it as $(A/B)_n$. A high-refractive-index layer was fabricated by dipping the PEN side of an ITO-PEN film, or the QCM, in PEI and TALH solutions several times alternately. Then PEI and SiO_2 solutions were used for the low-refractive-index layer. We fabricated five different nanoparticle ratios in composite samples: Type (i) was $(PEI/TALH)_3 + (PEI/SiO_2)_1 + (PEI/TALH)_2 + (PEI/SiO_2)_2 + (PEI/TALH)_1 + (PEI/SiO_2)_3$; Type (ii) was $(PEI/TALH)_6 + (PEI/SiO_2)_6$, which had the same dipping time; however, the order was different for making anti-reflections films composed of a gradient or a stepwise refractive index; Type (iii) was $(PEI/TiO_2)_6$; Type (iv) was $(PEI/TiO_2)_6$; and Type (v) was only a buffer layer. Every sample was optimized when they exhibited the highest transparency[6]. We also classified these samples as follows: Type (i) was six block layers; Type (ii) was two block layers; and Type (iii) and Type (iv) were one block layer.

2.3. Overview and flow chart for QCM-D

A schematic of the QCM/Unix system is shown in Fig 1. The QCM (10 MHz reference frequency) was connected to a Hartley oscillator and the frequency was monitored in one channel of a digital storage oscilloscope (GWINSTEK, GDS-1152A-U) set at 10 ms/div real-time sampling and 2M plot data storage. The QCM period was 100 ns and the oscilloscope was able to store plots over 80–400-ns periods, depending on the horizontal range of the oscilloscope. The stored analog QCM data was transferred to the Cygwin UNIX system. The 2M data set, which was composed of column1 (time t) and column2 (voltage V(t)), was analyzed and plotted with Gnuplot (http://www.cygwin.com, Red Hat, Inc.). We estimated the relative viscoelasticity of the fabricated films by calculating the decay time constant τ. Details of the data analysis programs (Program 1, 2 and 3) are in the supporting information. To calculate a constant Vmax value (see Fig 2), Program 1 was run. Then Program 2 adjusted the time origin to the damping start time. The decay time constant τ was calculated when the voltage was Vmax/e (e is Napier's constant) from Program 3.

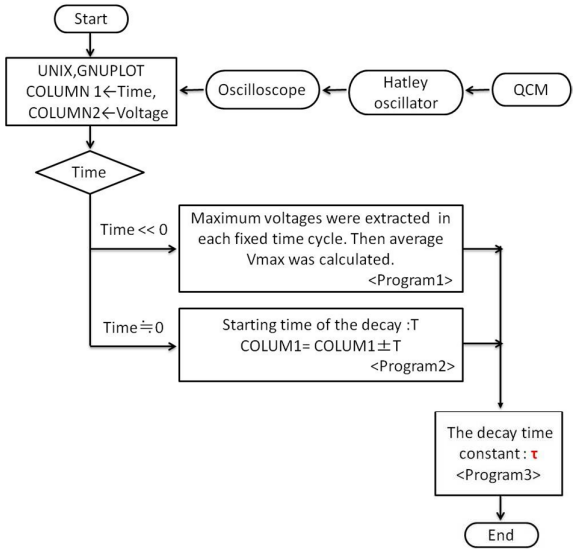

Fig 1. Flow chart of QCM-D, oscilloscope, and UNIX software. Nanoparticles and polymer were deposited on the QCM and measured with a Hartley oscillator and the digital oscilloscope. The oscilloscope stored 2M plots in a csv file format, which was transferred to a UNIX system for analysis by Program 1, 2 and 3. Graphics were drawn with Gnuplot.

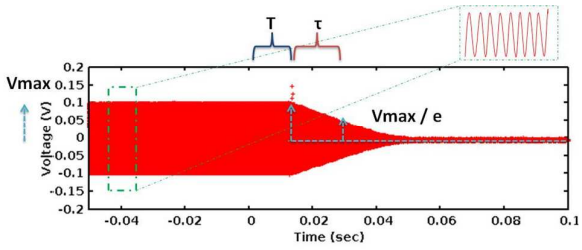

Fig 2. Raw QCM-D (attenuated amplitude) data. The vertical axis is voltage V(t) and the horizontal axis is time t. Vmax is the average of the maximum voltages over time (t<<0 region). The damping start time was not 0 sec, thus the origin was shifted to the damping start time "T". When the voltage was Vmax/e, the time was the decay time constant "τ".

2.4. Evaluation

The nanoparticle content ratios in the fabricated films were measured by QCM and GDOES (GDprofiler2, Horiba Scientific). GDOES is a rapid depth profiling technique for quantitative analysis. The viscoelasticity of the films was measured by QCM-D decay times as discussed above. The durability was checked by independent abrasion and bending tests. In the abrasion test, the films were subject to cotton swab abrasion at 10 g/cm^2 force. Parallel transmittance was measured with a haze meter (NDH5000, Nippon Denshoku Industries Co., Ltd) while the abrasion cycle was repeated 10–50 times. The difference in parallel transmittance before and after the abrasion was measured for an index of abrasion durability. To evaluate the bending durability, a 5-cm film was bent at an angle of 140° for 5 s. The durability was determined by the difference in parallel transmittance before and after bending.

3. Results and discussion

3.1. Nanoparticle content ratios

Schematic depictions of the fabricated films are shown in Fig 3 (a), and QCM data for the Type (i)–(iv) films are plotted in Fig 3 (b). As discussed above, the deposition cycles for Type (i) and Type (ii) created different refractive index structures. In Fig 3 (b), the frequency shift for the Type (i) film increased after rinsing, whereas it did not increase for the Type (ii) film. To analyze adsorption, we calculated the deposition of each layer by the frequency shifts. The frequency shifts of the cation and anion layers, the total frequency shift, and the nanoparticle ratios are given in Table 1. For Type (i) and Type (ii) films, the total frequency shifts were almost the same; however, the cation frequency shift was lower for Type (ii) and its nanoparticle ratio was high (91.1%). Type (i) had a nanoparticle ratio of (79.3%), which was the lowest of the films. We also found that Type (iii) had a nanoparticle ratio of 86.4%, while Type (iv) had the highest value (94.6%). In summary, the order of nanoparticle content ratios was Type (iv) > Type (ii) > Type (iii) > Type (i).

Nanoparticle content ratios were also estimated by GDOES in an Ar^+ etching mode, as shown in Fig 4 (raw data of GDOES was shown in supporting information Fig S2). We evaluated the intensity of each material as a function of depth; the interface between the film and substrate was indicated by the carbon (C) peak. The content ratio of each material was estimated by the integration of the peak areas up to the substrate interface. The nanoparticle ratios from GDOES (see Table 2) were different from those obtained by QCM; however, the order of nanoparticle compositions was the same, as shown in Fig 5. We also calculated the percentage difference in the values obtained from QCM and GDOES, defined as the difference between the two values divided by average. The results were: Type (i) 55.7%; Type (ii) 18.7%; Type (iii) 28.6%; and Type (iv) 43.3%. From the QCM (Table 1) and GDOES (Table 2) results and Fig 5, we concluded that the order of nanoparticle content ratio was Type (iv) > Type (ii) > Type (iii) > Type (i).

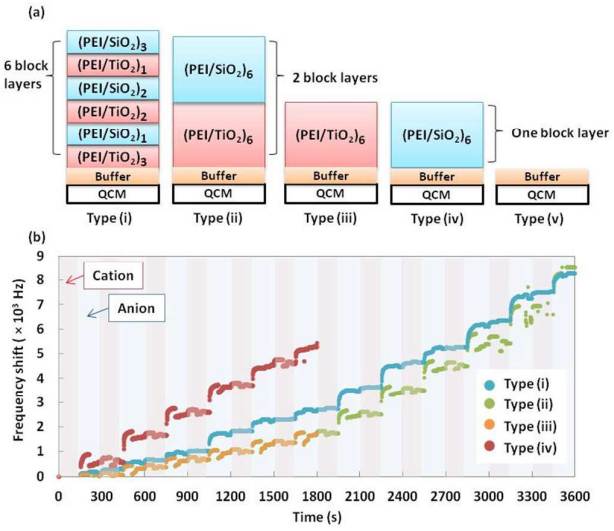

Fig 3. Frequency shift measurement by QCM. (a) Schematics of Type (i)–(v) films. The substrate was either the QCM or a PEN film. (b) QCM data for Type (i) (blue), Type (ii) (green), Type (iii) (yellow), and Type (iv) (red) films. The light-red zone corresponds to cation deposition for 1 min, followed by rinsing three times with water for 30 sec. The light-blue zone corresponds to anion deposition for 1 min, followed by rinsing three times with water for 30 sec.

Table 1. QCM frequency shifts and nanoparticle content ratios

Sample	Frequency shift (Hz)			Nano particle ratio (%)
	Cation	Anion	Total	
Type (i)	1719	6577	8289	79.3
Type (ii)	693	7076	7769	91.1
Type (iii)	267	1691	1958	86.4
Type (iv)	303	5315	5618	94.6
Type (v)	0	0	0	-

The nanoparticle ratio is given by the anion frequency shift/total frequency shift.

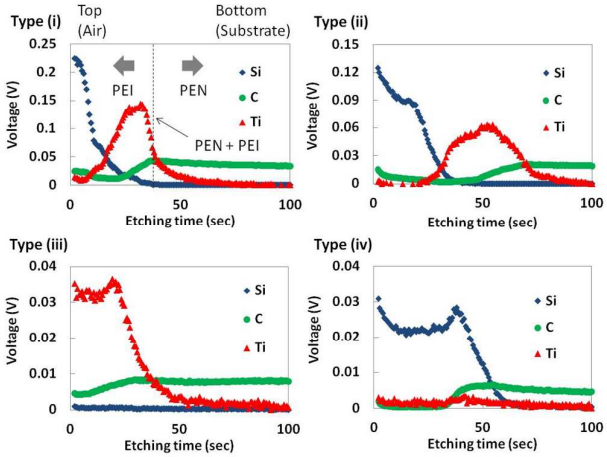

Fig 4. Depth of material distribution by GDOES profiling. We evaluated the depth of each material. We fabricated Type (i)–(iv) films on flexible PEN substrates. The interface between the fabricated film and substrate was at the C peak.

Table 2. Integral of voltages and nanoparticle content ratios from GDOES data

Sample	Integral of voltages (V)			Nano particle ratio (%)
	Si	Ti	C	
Type (i)	3.45492	4.4128	1.51574	83.84
Type (ii)	3.51693	3.25468	0.80182	89.41
Type (iii)	0.02493	1.30996	0.255054	83.96
Type (iv)	1.69593	0.1564	0.192346	90.59

Integral of voltages of Si, Ti and C are shown. The nanoparticle ratios were calculated from (Si +Ti) / (Si +Ti + C).

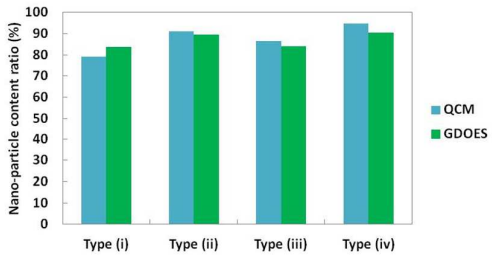

Fig 5. Estimation of nanoparticle content ratios from QCM and GDOES. The order of the nanoparticle content ratios was Type (iv) > Type (ii) > Type (iii) > Type (i).

3.2. Viscoelasticity

Digitized QCM-D plots for the Type (i)–(v) films are shown in Fig 6. The calculated Vmax, T, and τ values are listed in Table 3. Every sample exhibited shorter decay times than the Type (v) substrate sample. The decay times varied because of two factors: the nanoparticle ratio and the material depth distribution, which corresponded to the number of block layers. The Type (i) structure had multi-block layers and the lowest nanoparticle ratio (79.3% from QCM or 83.84% from GDOES). The Type (ii) structure also had multi-block layers, but a high nanoparticle ratio (91.1% or 89.41%). The Type (iii) structure had one block layer and a low nanoparticle ratio (86.4% or 83.96%). The Type (iv) structure also had one block layer, but the highest nanoparticle ratio (94.6% or 90.59%). From the QCM-D data, the decay time order was Type (i) < Type (ii) < Type (iii) < Type (iv). The Type (i) structure contained more polymer (see Table 3) and thus had the shortest QCM damping time because of greater energy absorbance by the soft material. The damping time of the Type (ii) film was longer than that of Type (i), which indicated that the former had a lower viscoelasticity. Despite the difference in decay times, the total frequency change for the two films was almost the same. This indicates that the nanoparticle ratio is a key viscoelasticity factor. Comparing Type (ii) and Type (iii) films, the orders of the nanoparticle ratio and decay times were different. The decay time was determined not by the nanoparticle ratio but by the layered structures (multi-block layers vs. one block layer). Type (iii) and Type (iv) were each made from one block layer and had different nanoparticle ratios. The order of the nanoparticle ratios was the same as that for the decay times. Thus, in this case, the decay time was determined mainly by the nanoparticle ratio. In summary, the decay times were longer, and the fabricated films had lower viscoelasticity, either because of the large quantities of nanoparticles or because of the uniform layered structure (one block layer).

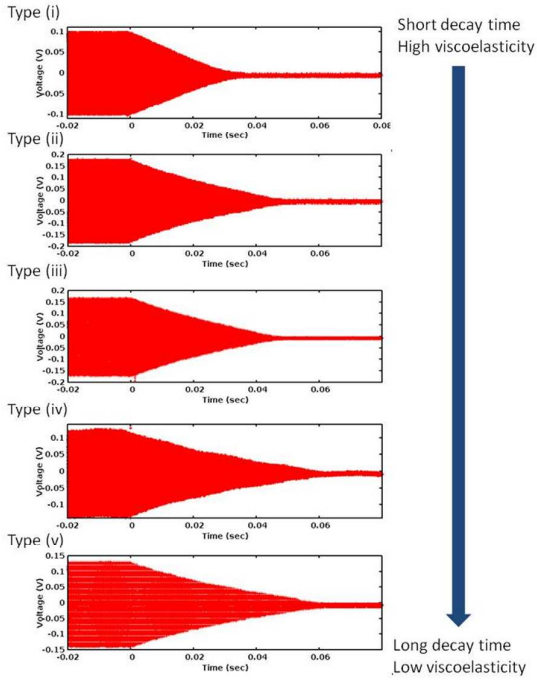

Fig 6. QCM-D for Type (i), Type (ii), Type (iii), Type (iv), and Type (v) films. Decay times correlated with the film viscoelasticities. Decay time constants τ were 0.0178012, 0.0239392, 0.024934, 0.0314432, and 0.0315996 for the Type (i)–(v) films, respectively.

Table 3. Decay time constant τ

Sample	Vmax (10^{-2} V)	T (10^{-2} sec)	τ (10^{-2} sec)
Type (i)	9.794	1.354080	1.78012
Type (ii)	18.484	-4.213160	2.39392
Type (iii)	17.995	10.092200	2.4934
Type (iv)	12.170	18.535040	3.14432
Type (v)	13.024	0.068000	3.15996

Calculated by Program 1, 2 and 3. The decay time constant τ was gradually longer from Type (i) to (v).

3.3. Abrasion durability

To characterize film durability, we performed abrasion tests. The film did not have strong durability if the transmittance was decreased by abrasion with a cotton swab at a force of 10 g/cm^2. As shown in Fig 7, the transmittance was reduced dramatically for the Type (i) samples (reduced to 89.6%). This film also had the lowest nanoparticle ratio and the highest QCM-D viscoelasticity. Type (ii) also did not have good durability (reduced to 97.6%), and it had a higher nanoparticle ratio relative to the Type (iii) film (reduced to 98.8%). This is most likely because of the two block layers in Type (ii). These multi-block layers were made either with SiO_2 or TiO_2 and PEI. Thus the difference in nanoparticle diameters affected the durability of the films. Type (iv) showed good abrasion durability (reduced merely to 99.5%), most likely because of the high nanoparticle ratio and one block structure.

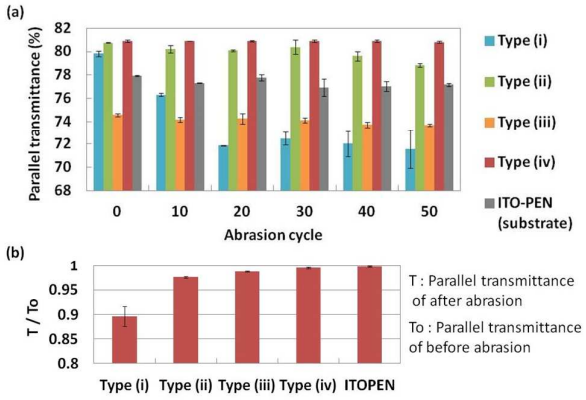

Fig 7. Abrasion tests. (a) The fabricated films were abraded with cotton swabs at a force of 10 g/cm^2. For abraded samples, the transmittance decreased because of film damage. (b) Parallel transmittance before and after 50 abrasion cycles produced decrements as shown. The average values of five points were used.

3.4 Bending durability

As shown in Fig 8, the flexibility of the films was characterized by the bending test. The Type (iii) and Type (iv) films exhibited the highest flexibilities (decreased to 98.1%, 98% transmission, respectively). In contrast, both the Type (ii) (decreased to 97.6%) and Type (i) (decreased to 97.2%) films had low bending durability. The bending durability was most likely affected by the polymer content ratio. Comparing Type (iv) and Type (iii), Type (iii) contained more polymer, and this influenced the bending durability. Although the Type (i) films had the highest polymer ratio, the bending durability was poor. This was because of the multi-block stacked structure with many interfaces of different materials and by having SiO_2 and TiO_2 nanoparticles with different diameters. Thus both Type (i) and Type (ii) had poor bending durability.

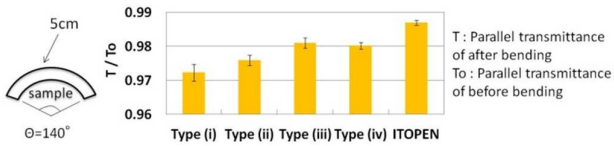

Fig 8. Bending tests to evaluate the flexibility of films. The 5-cm film was bent with angles of 140° as shown above. The flexibility was determined by the difference in parallel transmittance before and after bending. The average values from five points were used.

3.5 Relationship of viscoelasticity and durability

Above, we discussed the relation of viscoelasticity and durability of fabricated films with different nanoparticle content ratios. A flow chart is shown in Fig 9. Although the nanoparticle ratios of Type (ii) and Type (iii) films were different from the decay time order, the decay times correlated with the one block layer film or the multi-block stacked structures and the nanoparticle ratio. We also found that the films with high durability had long QCM decay times. Thus we conclude that longer decay times for polymer/nanoparticle stacked films indicate high abrasion or bending durability, and, by using QCM-D, we were able to estimate the durability of films without destructive tests. Thus, with the cost-effective QCM-D, digital oscilloscope, and UNIX system, we were easily able to measure the hardness of deposited films.

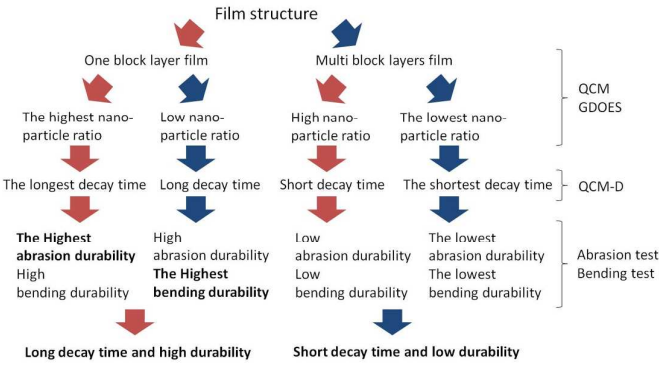

Fig 9. The relationship of QCM-D decay times and film durability. When the films had one block layer and a higher nanoparticle ratio, they had longer decay times and higher abrasion and bending durabilities. In contrast, when the film had multi-block layers and lower nanoparticle ratios, they had shorter decay times and lower abrasion and bending durabilities.

4. Conclusions

We fabricated polymer/nanoparticle stacked LbL films with PEI, TiO_2, and SiO_2 nanoparticles, with different nanoparticle content ratios. We then correlated the abrasion and bending durability of the films with QCM, QCM-D, and GDOES, and independent abrasion or bending tests. Decay times following QCM excitation were longer

when the films had one block layer and if there was a relative excess of nanoparticles. These films had high abrasion or bending resistance. Relative to the Type (iii)–(iv) films, the Type (i)–(ii) films had more block layers and a relatively low nanoparticle ratio; thus they exhibited shorter decay times and lower abrasion or bending durabilities.

In particular, we found that the abrasion and bending durabilities correlated with the decay times. By using QCM, QCM-D, and GDOES data, we can estimate film hardness, layered structures, and nanoparticle ratios using the relationship between QCM-D decay time and the abrasion or bending durability. These results also demonstrate that nondestructive analysis for an estimation of composite ratios and interface structures of layered films can be carried out by this simple experimental method.

Acknowledgements

We are deeply grateful to Ariyarit Atthaporn and Yosuke Tsuge whose helps made enormous contribution to our work.

Notes

The authors declare no competing financial interest.

References

1 D. Yoo, S. Shiratori and M. Rubner, *Macromolecules*, 1998, **31**, 4309-4318.
2 S. Shiratori and M. Rubner, *Macromolecules*, 2000, **33**, 4213-4219.
3 P. Paul, S. Lang, E. Yaseen, B. Peter, L. Jaebeom, M. Ashwini, K. Winardi, R. C. Mary, S. Max, K. John, L. Joerg and A. K. Nicholas, *Langmuir*, 2007, **23**, 7901-7906.
4 L. Zhang, Y. Li, J. Sun and J. Shen, *Journal of Colloid and Interface Science*, 2008, **319**, 302-308.
5 L. Zhang, Y. Li, J. Sun and J. Shen, *Langmuir*, 2008, **24**, 10851-10857.
6 K. Fukada and S. Shiratori, *Ind. Eng. Chem. Res*., 2015, **54**, 979-986.
7 G. Sauerbrey, *Zeitschrift für physik*, 1959, **155**, 206-222.
8 K. K. Kanazawa and J. G. Gordon, *Anal.Chem*, 1985, **57**, 1770-1771.
9 S. Bruckenstein and M. Shay, *Electrochim. Acta.,* 1985, **30**, 1295-1300.
10 A. B. Daniel and D. W. Michael, *Chemical Reviews,* 1992, **92**, 1355-1379.
11 N. Fukao, K. H. Kyung, K. Fujimoto and S. Shiratori, *Macromolecules,* 2011, **44**, 2964-2969.
12 Y. Kosaki, H. Izawa, S. Ishihara, K. Kawakami, M. Sumita, Y. Tateyama, Q. Ji, V. Krishnan, S. Hishita, Y. Yamauchi, J. P. Hill, A. Vinu, S. Shiratori and K. Ariga, *ACS Applied materials & interfaces*, 2013, **5**, 2930-2934.
13 B. Ding, J. Kim, Y. Miyazaki and S. Shiratori, *Sensors and Actuators B*. 2004, **101**, 373-380.
14 R. Michael, H. Fredrik, K. Anatol, B. Peter and K. Bengt, *Rev. Sci. Instrum*., 1995, **66**, 3924-3930.
15 R. Michael and K. Bengt, *Review of Scientific Instruments*., 1996, **67**, 3238-3241.
16 M. Rodahl and B. Kasemo, *Sensors and Actuators B,* 1996, **37**, 111-116.
17 M. Yang and M. Thompson, *Analytical chemistry*, 1993, **65**, 1158-1168.
18 S. J. Martin, G. C. Frye and A. J. Ricco, *Analytical chemistry*, 1993, **65,** 2910-2922.
19 M. Rodahl, F. Höök, C. Fredriksson, C. Keller, A. Krozer, P. Brzezinski, M. Voinova and B. Kasemo, *Faraday Discussions,* 1997, **107**, 229-246.
20 F. Höök, M. Rodahl, P. Brzezinski and B. Kasemo, *Langmuir*, 1998, **14,** 729-734.
21 C. Fredriksson, S. Kihlman, M. Rodahl and B. Kasemo, *Langmuir*, 1998, **14,** 248-251.
22 L. Charlotte, R. Michael and H. Fredrik, *Anal. Chem*., 2003, **75**, 5080-5087.
23 M. T. Julianne, L. O. Laura, R. K. Thomas, S. M. Eric, H. Dehong, E. L. Samuel, C. M. Arielle, D. Merve, M. V. Ariane, D. T. Marco, E. Eseohi, R. W. Stephanie, F. Li, R. A. Christopher, Z. Zihua, W. Hongfei, O. Galya, J. M. Catherine, J. H. Robert, A. P. Joel and M. G. Franz, *J. Phys. Chem. C.,* 2015, **119**, 534-546.
24 D. W. Joshua, A. H. Ben, J. M. Timothy, E. Steve, B. W. Grant and J. W. Erica, *Phys. Chem. Chem. Phys.,* 2015, **17**, 3880-3890.
25 X. Su, Y. J. Wu, R. Robelek and W. Knoll, *Frontiers in Bioscience*, 2005, **10**, 268-274.
26 P. D. Aleksandra, M. Agnes, J. Luc, R. Michael, C. Arkadiusz, H. Fredrik, N. Tommy and S. Emma, *Nanoscale*, 2015, **7**, 583-596.
27 M. V. Voinova, M. Rodahl, M. Jonson and B. Kasemo, *Phys. Script*, 1999, **59**, 391-399.
28 F. Jiajie, Z. Tao, S. Jie, J. Zhongying and M. Yuqiang, *Scientific Reports,* 2015, **5**, 8491.
29 A. H. Hauke, T. Nicolas, G. Viktoria, K. Bengt and G. Michael, *Phys. Chem. Chem. Phys*., 2012, **14**, 9037-9040.
30 H. S. Hsin, L. L. Denisse, S. Takuya, J. B. Matthew, N. Nicholas, L. Jingxiong, A. H. Stephen, T. Khershing, S. Joel, T. W. Chaille, K. B. Susan, L. M. Lisandra and L. Trevor, *Nature Communications*, 2014, **5**, 5078.
31 S. Lei, S. Jelmer, K. S. Prashant, J. K. Hans, C. V. D. M. Henny and J. B. Henk, *ACS NANO*, 2014, **8**, 8457-8467.
32 W. Yinan, K. Yohei, L. Yang and N. Ravin, *ACS Appl. Mater. Interfaces.,* 2015, **7**, 1652-1661
33 C. A. Keller and B. Kasemo, *Biophysical Journal*, 1998, **75**, 1397-1402.
34 D. Jelena, A. Selver, M. T. Nicole and L. W. Stephanie, *Langmuir,* 2015, **31**, 721-731.
35 A. J. Joshua, R. T. Seyed, Z. Zhilei, Y. Saziye and J. C. Nam, *ACS Appl. Mater. Interfaces.,* 2015, **7**, 959-968.
36 W. Andreas and T. Nathalie. *Anal. Chem*., 2014, **86**, 8017-8020.
37 L. Cuixia, Z. Enzhong, W. Tao, S. Weixiang, L. Xinxing and T. Zhen, *J. Phys. Chem. B,* 2015, **119**, 612-619.
38 C. Xiao, Y. Jingfa, L. Guangming and Z. Jiang, *Soft Matter*, 2014, **10**, 5568-5578.
39 T. Wen, M. P. Gina, H. Geng, G. Kai, Z. Jinjun, W. Chrys, L. D. Gary and L. B. Matthew, *J. Am. Chem. Soc.,* 2014, **136**, 16357-16367.
40 X. Man, J. Jing and Y. Z. Bao, *RSC Adv.,* 2014, **4**, 38943-38950.
41 H. Yu, J. Jing, H. Yuanyuan, Y. Jinghua, J. Wei and L. Haojun, *RSC Adv*., 2014, **4**, 7716-7724.
42 B. Torun, C. Kunze, C. Zhang, T. D. Kühne and G. Grundmeier, *Phys. Chem. Chem. Phys*., 2014, **16**, 7377-7384.
43 A. Lana, W. Shengqun, X. Zhenghe and M. Jacob, *J. Phys. Chem. C*., 2011, **115**, 15390-15402.
44 F. F. Antonio, C. E. Nicel, M. F. Timothy and C. A. Rigoberto, *ACS Applied Materials & Interfaces*, 2010, **2**, 3726-3737.
45 N. Tiina, P. Hanna, Ö. Monika, P. Jouni and L. Janne, *Cellulose*,

2012, **19**, 779-792.
46 X. C. Hui, P. Y. Swee, S. O. Mohamed, L. A. Abdul and L. JitKang, *ACS Appl. Mater. Interfaces.,* 2014, ***6***, 16508-16518.
47 C. V. L. Reid, R. Maria, H. J. S. Paulo, A. Patrizia, R. Javier, V. Kislon, S. Francesco and A. K. Alfredo, Nature Communications, 2014, **5**, 4482.
48 T. P. Joseph, E. S. Benjamin, K. R. Dariya and L. L. Jodie, *Soft Matter*, 2014, **10**, 8107-8115.
49 W. Qiaoying, W. Zhiwei, Z. Jie, W. Jie and W. Zhichao, *RSC Adv*., 2014, **4**, 43590-43598.
50 K. Olga, S. Majid, D. Andra and M. C. Per, *Langmuir,* 2013, **29**, 9551-9561.
51 J. Pisonero, B. Fernandez, R. Pereiro, N. Bordel and A. S. Medel, *Trends in Analytical Chemistry,* 2006, **25**, 11-18.
52 P. Jorge, *Anal Bioanal Chem*, 2006, **384**, 47-49.
53 D. M. Ritchie and K. Thompson, *Communications of the ACM*, 1974, *17,* 365-375.
54 L. Yuri, A. Katsuhiko, O. Mitsuhiko, I. Izumi and K. Toyoki, *Langmuir,* 1997, **13**, 6195-6203.

A graphical and textual abstract for the Table of contents entry